Received: 9 April 2023 | Revised: 16 August 2023 | Accepted: 17 August 2023

DOI: 10.1111/jmi.13217

Journal of Microscopy RMS

THEMED ISSUE ARTICLE

Work smart, not hard: How array tomography can help increase the ultrastructure data output

Irina Kolotuev

Electron Microscopy Facility, University of Lausanne, Lausanne, Switzerland

Correspondence
Irina Kolotuev, Electron Microscopy Facility, University of Lausanne, Lausanne 1015, Switzerland.
Email: irina.kolotueva@unil.ch

Abstract

Transmission electron microscopy has been essential for understanding cell biology for over six decades. Volume electron microscopy tools, such as serial block face and focused ion beam scanning electron microscopy acquisition, brought a new era to ultrastructure analysis. 'Array Tomography' (AT) refers to sequential image acquisition of resin-embedded sample sections on a large support (coverslip, glass slide, silicon wafers) for immunolabelling with multiple fluorescent labels, occasionally combined with ultrastructure observation. Subsequently, the term was applied to generating and imaging a series of sections to acquire a 3D representation of a structure using scanning electron microscopy (SEM). Although this is a valuable application, the potential of AT is to facilitate many tasks that are difficult or even impossible to obtain by Transmission Electron Microscopy (TEM). Due to the straightforward nature and versatility of AT sample preparation and image acquisition, the technique can be applied practically to any biological sample for selected sections or volume electron microscopy analysis. Furthermore, in addition to the benefits described here, AT is compatible with morphological analysis, multiplex immunolabelling, immune-gold labelling, and correlative light and electron microscopy workflow applicable for single cells, tissue and small organisms. This versatility makes AT attractive not only for basic research but as a diagnostic tool with a simplified routine.

KEYWORDS

array tomography, blood cells, diagnostic vEM, histology, model organisms, SEM, volume electron microscopy

1 | INTRODUCTION

Ultrastructural studies of cells, tissues and even whole organisms have vastly improved our understanding of the processes that make cells 'tick'. High-resolution ultrastructural analysis can only be carried out with electron microscopy (EM), but these approaches have limitations. For example, Transmission Electron Microscopy (TEM) techniques have been indispensable for understanding cell biology and cell architecture at the subcellular level. However, except for some high-end examples, this technology is limited by its small field of view (FOV), defined by the limitation of commercially available microscopes. In addition, due to the nature of the electron beam

and sample preparation, TEM does not easily provide three-dimensional (3D) information, which can make image analysis and interpretation problematic. Various EM methods and techniques have emerged in recent decades to address these problems, most of which can be attributed to improved high-performance field emission Scanning Electron Microscopes (SEM).[1,2] The advantages of novel backscattered electron detectors and modern SEM columns have transformed sample analysis, providing the previously unattainable resolution-to-area ratio. The most notable innovations in 3D-EM imaging techniques were the introduction of serial block face (SBF)[3] and Focused Ion Beam (FIB) techniques.[4,5] Around the same time, the field also saw the emergence of array tomography (AT) initially developed for multiplex fluorescence analysis.[6,7] This approach has increasingly been used to facilitate the ultrastructural analysis of cells and tissues.[8,9] Together with the on-tape collection method[10,11] AT on large support rapidly emerged as an additional volume EM (vEM) technique. These three SEM-based techniques differ mainly according to the manner used to expose the sample surface. Each technique has advantages and disadvantages, and it is essential to consider these issues when selecting the method to answer a given biological question.[1,12,13] Specifically, several aspects should be considered, including (1) the sample area and total volume that can be acquired in a given run, (2) the requirements for z resolution, (3) the ease of Region of Interest (ROI) identification, (4) optimal resolution to observe the biological structure relevant for the study and (5) the possibility of reimaging the samples.

Many manuscripts and reviews cover the pros and cons of these approaches.[12,14,15] Although there is value in discussing the ideal sample preparation and imaging approach, these debates have obscured the true revolution: *SEM can efficiently replace TEM* to address many cell and developmental biology questions! A range of existing TEM techniques is seldom incorporated into the required training of cell and developmental biologists since it involves a steep learning curve. In contrast, the operation of a scanning microscope is much more intuitive than a transmission microscope, with comparable purchase and maintenance costs, making this technology accessible to researchers working in various fundamental and applied fields.

Here, I will focus on AT in its 3D context. This procedure utilises a large boat diamond knife, physical sectioning, and the manual collection of sections on a large support (e.g., silicon wafers or glass slides) to prepare a sample that SEM can analyse. Unlike other vEM procedures, AT requires minimal investment to start the experiments when the appropriate SEM is available. Additional techniques have emerged in recent years to facilitate the collection of multiple sections on such a support, each using a slightly different collection and transfer strategy.[10,16–20] The method is easy to master in comparison to any other EM method. Surprisingly, despite its clear benefits, it has not been extensively used in research and even less as a medical diagnostic tool.

In this manuscript, I draw on over a decade of first-hand experience to discuss the benefits and possibilities of AT.[19,21–29] Through a series of examples used to highlight the specific strengths of AT-SEM, I hope to initiate a more extensive discussion about how this true SEM revolution can expand access to electron microscopy beyond the committed EM specialists to allow researchers as well as clinicians to gain insight into the ultrastructural changes in cells, tissues and even organs. The hope is that it can help to 'democratise' electron microscopy for all.

2 | METHODS AND RESULTS

2.1 | Background

The aim is not to give a detailed methodology of the AT sample preparation, as it can be found in numerous methodology manuscripts.[19,30–32] Instead, this manuscript aims to address different misconceptions regarding AT sample preparation and, by providing practical examples, highlight the potential for analysing biological samples. I concentrate on key workflow steps and questions that show how, with the help of AT methodology, various issues that complicate other EM approaches can be addressed. Like other EM techniques, AT is a multistep procedure. Therefore, when discussed, it must be broken down into separate steps, which have their unique challenges: sample preparation and embedding, trimming and sectioning, imaging and analysis. These steps should be considered as independent parts with fundamentally different requirements and must be executed accurately; failure in one step can cause the whole workflow to fail. In this article, I concentrate only on the AT techniques that do not require special equipment for section generation (apart from a dedicated diamond knife) and require the analysis of <1000 sequential sections.

2.2 | Sample preparation

Good sample quality and preparation are prerequisites for any successful EM experiment. The beauty of AT is its compatibility with almost all resin-based preparations. Without exaggeration, any generic EM procedure should be suitable for analysis by AT, including chemical and microwave fixation and High-Pressure Freezing-Freeze Substitution preparation. The choice of heavy metal steps

is also very flexible. Unlike the situation with SBF/FIB-SEM, if it is necessary to improve the contrast of the sections, it can be quickly done directly on sections.[19,26] Yet, depending on the microscope, standard osmium-Epon procedure might not require this step altogether.

2.3 | Embedding

EM operates under vacuum conditions, so the soft biological material (e.g., cells and tissues) must be dehydrated and hardened by embedding in polymer resin. There is no special resin requirement for AT, as thin sections exhibit minimal charging (a typical problem for nonconductive SEM samples that interact with the electron beam), even without additional grounding. This flexibility frees AT from the constraints of special resin requirements, as practically any block type that is compatible with diamond knife sectioning can be used for the procedure. Further, standard moulds are ideal for pellets of cells, bacteria and samples that do not require a particular orientation. Flat embedding is preferable if the sample is polarised or if a specific ROI must be identified. These blocks can be analysed under a binocular or light microscope to localise a precise ROI to ensure the correct trimming and subsequent ultrathin sectioning orientation.[33]

Thus, the flexibility of AT is such that there is no special requirement for the preparation of the sample, and even existing blocks can be analysed or re-analysed by it. The examples presented in this manuscript were selected from a collection of blocks spanning the last two decades that I had prepared for TEM observation in various studies.

2.4 | Block shaping and trimming

The polymerised block is composed mainly of empty resin, with the sample occupying only a small part of its volume (Figure 1Ai). Therefore, it is essential to expose the sample area by trimming the excess resin from the sides and the leading face surface of the block (Figure 1Aii). The trimming step minimises the area in contact with the delicate diamond knife edge and reduces potential damage through wear. A razor blade is often used to trim the surface into a pyramid shape with the top and bottom edges of the block lying parallel. The idea of top and bottom sometimes is confusing since, in many cases, there are no significant differences between the top and bottom of the block. However, when installed inside the ultramicrotome, the upper part of the block relative to the microtome binocular is referred to as the top. According to this orientation, the rest of the sides are designated accordingly (Figure 1B and C). In addition to the sides, the block face must be flattened to enable the maximal parallelism between it and the ultradiamond knife blade. The step of aligning the block and the diamond is often slow and prone to mistakes, with a high risk of damaging the knife.

Block shaping and trimming are among the more challenging steps to master. The ability to make a neat pyramid with two parallel edges, a smooth block face and its alignment with the diamond knife tends to define a good ultramicrotomist. The main reason is that it requires patience, practical experience and adaptation to counterintuitive manipulations of the ultramicrotome gears. However, a more intuitive solution is often overlooked: a robust diamond trimming tool (Diatome, Switzerland), which efficiently polishes the surface of the sample block to produce an unambiguous reflection pattern (Figure 1D, arrow to resin debris). It can also achieve perfect edge parallelism of the block sides (Figure 1E; Supplementary Movie 1a). The procedure is rapid even when a complete run of the microtome arm (~200 μm) is required since it is performed at a maximum sectioning speed and section thickness of 500 nm. Blocks trimmed this way are precisely parallel to the blade in the front and top/bottom orientations, which tends to be challenging to achieve with manual trimming (Figure 1F). The reflection of the backlighting from the ultramicrotome is a prerequisite for a successful thin-sectioning step, and the straightforward achievement of this step dramatically facilitates the initial effort (Figure 1G, arrow to the light on the block face). The presented workflow is the manner I found the most efficient through trial and error.[27] However, the trimming step can be adapted to the experimental habits of the operator, who might find other methods more appealing.

2.5 | Sectioning and array generation

With TEM, the overall FOV is limited to a maximum of 3 mm diameter (the size of the sample holder) and a sample thickness typically below 300 nm (depending on the TEM accelerating voltage). The ultrathin sections for TEM analysis are generated with the help of the diamond-blade knife mounted on a metal recipient basin filled with water (Figure 1H, Ultra 35°, Diatome, Switzerland). Newly cut sections float on the water surface one after another and remain stretched and attached in the order in which they were cut (Supplementary Movie 1b). The sections are transferred from the knife basin onto a dedicated sample support, a grid of a uniform 3 mm diameter shape that comes in different shapes in its central part (Figure 1I). The grids with dried sections attached on their surface are introduced into the TEM via a special holder for routine TEM or TEM-tomography analysis (Figure 1J, arrow). Many tissue sample sections are transferred on relatively

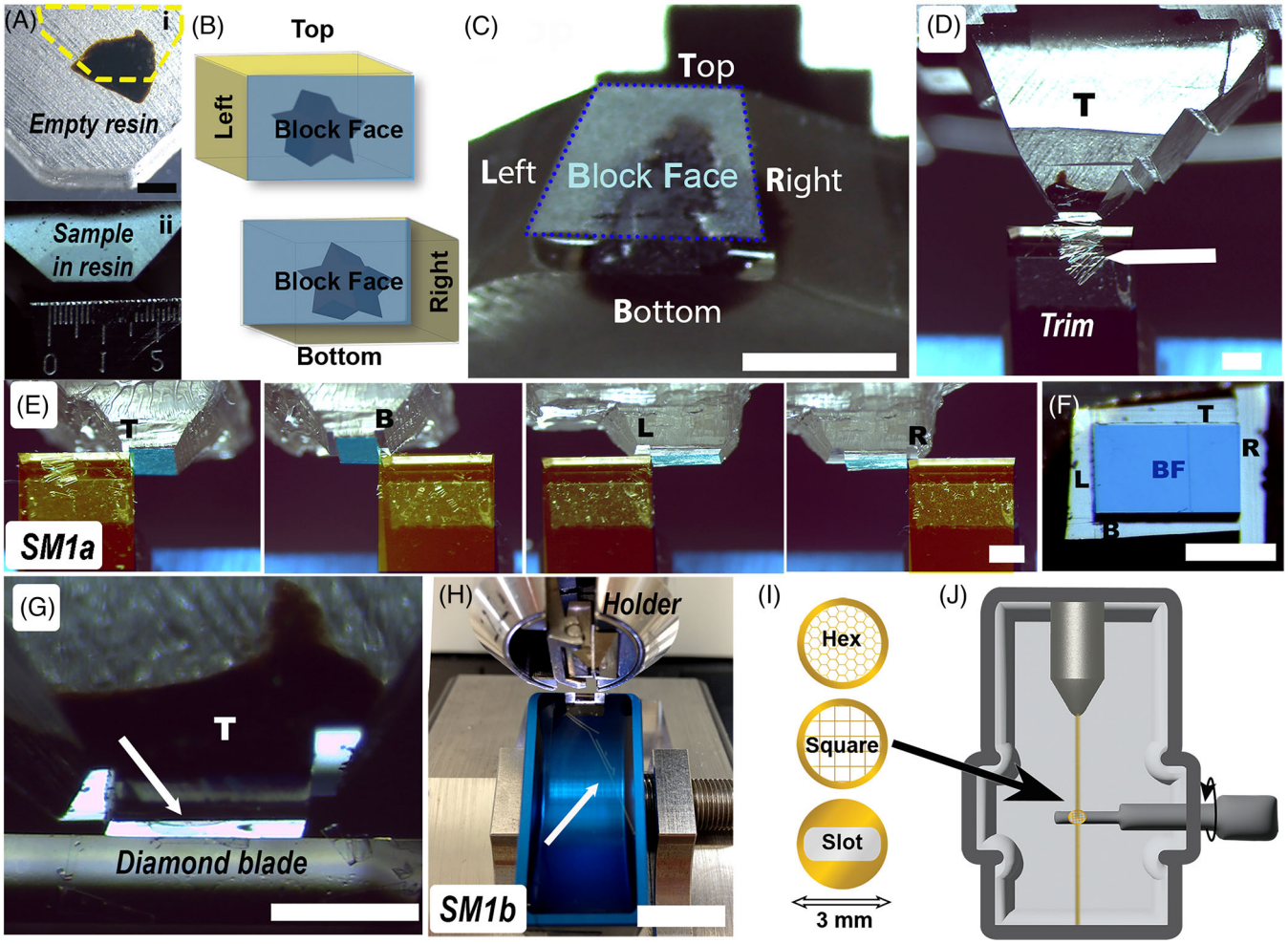

FIGURE 1 Sample trimming and preparation for thin sectioning. (A) A typical polymerised resin block (transparent) with processed tissue (brown). The dotted line in (i) delimits the portion of the sample that will be preserved after rough trimming (ii). A razor blade trims the empty resin around the sample to expose the tissue that will be shaped to the tiny surface dedicated to sectioning. Scale bar: 1 cm. (B) A schematic drawing of a rectangular resin block with a star shape representing a sample inside. In many cases, there is no particular importance to the block's orientation; nevertheless, it makes sense to establish a nomenclature for the procedural description. In this way, the *top* and *bottom* edges of the block refer to the position inside the ultramicrotome holder related to the upper and lower portions of the ultramicrotome. *The block face* is the frontal interface between the block and the diamond knife blade. *Left* and *right* correspond to the operator's position in front of the ultramicrotome. (C) Front view of hand-trimmed block shaped as a trapeze with parallel top and bottom surfaces. Block face perimeter marked by dotted line represents the surface ready for ultrathin sectioning. Scale bar: 500 μm. (D) 90° trim diamond set on the ultramicrotome in the position to trim the block face of the sample. The arrow points to the resin shavings generated during trimming. Scale bar: 1 mm. (E) A sequence of images summarising sample trimming using the 90° trim diamond trim. The opposite sides of the blade are parallel; thus, the opposite surfaces of the trimmed block will be parallel. If the sample is rotated 90° and the procedure is repeated, all four surfaces will be parallel. A similar effect of parallel opposite surfaces can be achieved with 20° and 45° trims. Scale bar: 1 mm. (F) The face view on the block after diamond trimming. The light blue part traces the previously hand-trimmed portion. The dark blue rectangle, the block face area trimmed with the trim diamond 90° blade. Scale bar: 500 μm. (G) Block face of the sample from panel D, aligned to the sectioning knife, arrow points to the bright line indicating the region where the bottom light from the ultramicrotome reflects on the block face surface (arrow). The diamond blade is aligned to be parallel to the top and bottom edges of the block. Scale bar: 500 μm. (H) Regular ultradiamond knife (blue) installed on the microtome. The sample is fixed on the holder, which is fixed on the microtome specimen arm. The knife basin is filled with water, and the sections float on its surface (arrow). Scale bar: 1 cm. (**I**) Schematic drawings of different types of TEM grids. The outer diameter of the grid is uniform (3 mm); however, the inside part varies according to the experimental needs. (**J**) Schematic drawing of the internal part of the TEM microscope with a grid inside (arrow). If tomography is used, the holder is rotated on its axis (circular arrow).

robust square or hexagonal mesh grids, but the grid bars can obscure parts of the FOV. Film-coated slot grids solve this problem at the cost of increased fragility and more challenging manipulation. For serial sectioning, an additional level of complexity is presented: sequential sections must be transferred in order without loss. Acquiring such competence involves a steep learning curve and a high failure rate initially, often proving to be the breaking point for novices.

Different SEM-based microscopy techniques were developed as an incentive to alleviate TEM preparation-related problems, of which I will cover only three (Figure 2A). In FIB and SBF-SEM, the sample is set inside the SEM chamber, and its surface is gradually exposed by physical sectioning with the built-in ultramicrotome (SBF) or shaved off with a gallium ion beam (FIB). Then, the newly exposed surface is scanned to obtain its image. After multiple iterations of the complete cycle, a 3D EM stack is generated with high stability and minimal section distortions. Some limitations balance the strength of these approaches: it is impossible to change the contrast load of the sample after the embedding, and if it is insufficient, the chances of acquiring a quality dataset are minimal. Another drawback is the impossibility of reimaging the same area with different acquisition parameters or imaging a different, adjacent area, as these techniques are destructive. AT manages to overcome some of the limitations of TEM or FIB/SBF. For example, compared to TEM, the ultramicrotome sectioning and transfer of multiple sections to a large substrate used in AT is easier and enables larger numbers of sections to be collected. Specifically, the flat conductive surfaces such as coated glass slides/coverslips or silicon wafers used in AT are more forgiving than on-grid transfer used in TEM, as it does not require the same level of dexterity. Compared to FIB/SBF-SEM, subsequent imaging can be done on numerous ROIs by AT, with different image field sizes or resolutions, and can be coupled to enhanced contrast or immunolabelling. However, the alignment of the acquired images can be problematic, similar to the ssTEM: manual or semimanual alignment can be challenging due to the distortion of some sections.

Various strategies have been developed for AT sectioning/transfer, and the choice of technique will depend on the sample type, project goal and available equipment. To generate AT arrays, I use an ultra ATS diamond knife (Figure 2B; Diatome, Switzerland), as it is equipped with a large boat that allows the handling and transfer of longer ribbons on the large support. The consecutive sectioning can run as long as the length of the basin permits (Figure 2B, Supplementary Movie 2a). The water is drained from underneath by active drafting through a syringe or by passive dripping (Figure 2B, blue arrow). The bottom of the basin is flat to maintain the wafer in a horizontal position, the draining does not create turbulence and the ribbons can be organised with better flexibility. Slow evaporation favours the relaxation of the sections (Figure 2C, Supplementary Movie 2b).

Section thickness for TEM has been adapted to the electron-beam penetration capability and has increased from ~60 nm thick in regular TEM to ~300 nm in TEM tomography. SEM imaging is independent of the section thickness limitations as the information is collected from the sample's surface. The exact depth from which the information is collected depends on the detector and electron-beam parameters. Sectioning within the 50–300 nm range is achievable with the ultra ATS knife and acceptable for most cell and developmental biology questions. When transferred to the wafer, the section's light interference colour corresponds to different thicknesses, as indicated on the wafers (Figure 2D). The familiar colour of floating sections that represent a particular thickness in water differs from when the sections dry and attach to the wafer. Optimal section thickness should be determined based on the relative size of the structure of interest within the sample volume. For smaller structures like vesicles, section thickness should be chosen according to the size of its fraction: a 50 nm structure will require sections of <25 nm to capture at least one structure per section. For the tissue architecture analysis featuring cells of 5–10 μm size, the thickness of the section should be between 80 and 200 nm. Careful experimental design is a prerequisite to efficient volume generation and image acquisition.

Even though the general goal is to obtain straight and continuous ribbons of sections, the sample and the environmental conditions can make this challenging. Some ribbons, indeed, will be straight and attached from the beginning. Nevertheless, in many cases, they will curve no matter how well they are trimmed or will not stay intact after drying, even though they were initially attached (Figure 2D). As I will show below, in most cases, the shape of the ribbon does not pose a significant problem, and the significance of the ribbon's intactness will be related to the project goal.

2.6 | Minimal time, maximal efficiency: lateral screening

TEM-grid screening is tedious, particularly when a specific ROI must be located, as it requires frequent transitions between low and high magnification. For ssTEM, screening multiple grids and combining the information into a volume can quickly become challenging due to a large number of grids. When using FIB/SBF, the ROI must be located in 3D, which is not a straightforward endeavour,

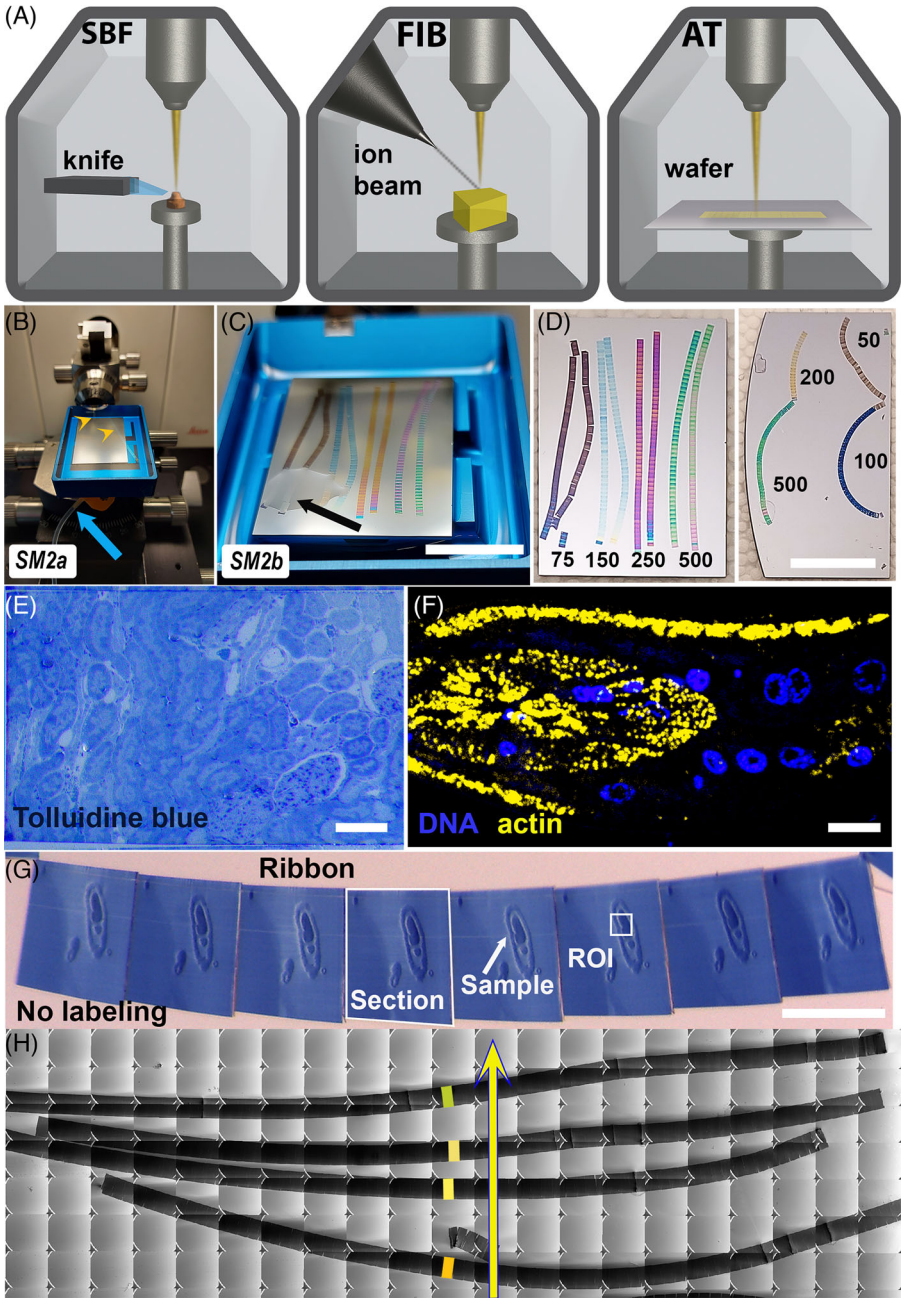

FIGURE 2 Sample preparation for AT and array generation. (A) Schematic drawing of different types of SEM acquisitions inside the generic SEM chamber. For the SBF, the sample is thinned by the diamond knife of an inbuilt ultramicrotome. For the FIB, the sample's surface is shaven away by a beam of gallium ions. This way, the sections in SBF and FIB disappear after one acquisition round. The AT samples are sectioned and transferred on the wafer outside of the SEM, allowing AT sections to be reimaged multiple times in multiple independent iterations. (B) Top view of the ultramicrotome with ultra ATS knife filled with water and a 2 × 4 cm wafer piece placed inside. A trimmed sample is aligned with the knife edge. The needle of the syringe to draft water is attached below (blue arrow). The ribbon of sections (array) floats on the water surface (arrowheads). (C) Air-drying of the wafer after the retraction of water. This step is a prerequisite for successful section transfer and crucial for avoiding the creation of major- and mini-folds. This step should not be rushed; patience is advised to allow all water to evaporate gradually (arrow, Supplementary Movie 2b). The thickness of the sections was changed during the same sectioning. This results in ribbons of different thicknesses producing a distinct interference colour. Please, note exact colours differ in wet and dry environments. Scale bar: 1 cm. (D) Wafers with ribbons of dried sections with different interference colours. Numbers alongside the ribbons indicate the thickness of the sections (determined by the microtome). Brown = 50 nm, Deep blue = 100 nm, Light blue = 150 nm, Yellow-golden = 200 nm. The ribbon's integrity depends on the sample's nature and sectioning conditions. Scale bar: 1 cm. (E) AT workflow does not require toluidine staining for ROI localisation. However, a representative section from the toluidine blue staining can be analysed with brightfield/phase imaging for different histology-related questions if necessary. Scale bar: 100 µm. (F) Fluorescence imaging of *C. elegans* sections labelled for DNA (Dapi, in blue) and actin (B-actin, in yellow). Scale bar: 1 µm. (G) After wafer drying, sections can first be

and it often results in either missing the ROI or acquiring unnecessarily large areas to increase the chance of capturing it. These limitations result in excessive investments of time and money, which frequently cannot be justified for complex projects.

To facilitate ROI localisation in both *XY* and *Z* planes, the AT sections on a wafer can be prescreened by labelling some sections with a histology stain such as toluidine blue (Figure 2E), or a fluorescence immunolabelling for multiplex labelling or correlative procedure (Figure 2F). Generating a comprehensive map of each wafer begins with proper documentation of sample orientation at the trimming step during the sectioning that provides information regarding the *x*–*y* expectations of the sectioned sample, section thickness and section number (*z*-depth). Thus, simply using the reflection mode of the binocular without staining, it is possible to have general information regarding the sample, as ribbons of sections are visible as well as individual sections, the presence of the sectioned sample inside the empty resin, and even the presumable location of an ROI (Figure 2G). The sections are collected sequentially in a linear ribbons, and ribbons can be ordered to generate a sequential array. The dried support can be directly analysed using SEM. With or without labelling, the position of sequential sections on the support itself serves as a map for quick and efficient localisation of the ROI.

ROI localisation can be achieved by a *lateral screening strategy* that helps to accomplish localisation procedures with minimal effort. SEM examination of the sections on support at low magnification generates a preliminary map, which is helpful for manual or automatic data acquisition.[27] To facilitate map generation, SEM manufacturers offer a software option to acquire low-magnification maps. After generating the map, the ribbons on the wafer are scanned starting at a random position around its centre (Figure 2H, yellow). This 'anchor' section is carefully analysed to assess the distinct features of the sample quality, the overall ROI and the particular parts. If there are several ribbons, the procedure is repeated for all ribbons on a given wafer (Figure 2H, yellow arrow). As the arrays are sections acquired in sequence, such assessment provides the details necessary for the operator to conclude what to expect from the adjacent sections upstream and downstream of the 'anchor'. For longer ribbons or samples with faster changes in topography, more than one 'anchor' section can be sampled for each ribbon, preferably at regular intervals.[19] Subsequently, selected regions can be imaged with higher acquisition parameters to narrow down the sequences to be analysed with higher resolution. Once an ROI has been identified, it can be interpreted in detail using appropriate acquisition parameters in manual or automatic mode. The choice of approach will largely depend on the nature of the sample and the question to be addressed, together with the available equipment.

2.6.1 | What and how: Using AT without fear

Whatever screening strategy is selected, the image quality will depend on the prepared sample's quality, the given microscope's capabilities and the chosen imaging mode. However, several points should be kept in mind: (1) the working distance to the detector typically ranges from 2 to 4 mm, with the optimal distance defined by the manufacturer, (2) different combinations of settings for the accelerating voltage and beam current should be tested before starting the experiment, to identify the best parameters, (3) the speed of acquisition and the size of the frame will define the resolution of the image and its size, and (4) different detectors will collect electrons from different depths of the section, so using several detectors can provide additional information when imaging thicker samples.

To illustrate the strength and flexibility of AT-SEM, five samples in this manuscript were chosen from the collection of previous experiments prepared for TEM needs. No practical scientific reason was in mind, only the idea to illustrate the point and the likelihood of encountering an analogous situation in likewise samples. The examples cover the specimens embedded in different resins (HM20, Durcupan, Epon-Araldite), and the biological samples presented include bacterial pellets and cell suspensions, cell monolayers, tissues prepared for morphological or immunolabelling workflow, and simple, nonhomogeneous organisms. They were sectioned and transferred on ~2 × 4 cm bits of a silicon wafer and SEM-imaged to make a specific point in each case, demonstrating the potential application of the AT approach for similar experimental studies. Due to space limitations, describing the underlying biological background for each example is impossible. I will concentrate on the ultrastructure and image quality within the context of each case

prescreened using the reflected light even before mounting the sample for SEM analysis. The overall state of the sample can be assessed already at this point. The hierarchy used for the AT samples is graded as: Wafer→ Ribbon→ Section→ Sample→ ROI. Scale bar: 500 μm. (H) Tiled image of a wafer acquired with ETD-SE to illustrate the idea of lateral screening. The sampling begins in the middle of the first ribbon and progresses not to the beginning and the end section of the next array but leaps to the middle portion of the following array. This way, the information regarding the overall state of the sample on different ribbons can be easily achieved. Such an approach is even more crucial for analysing nonhomogenous samples with variable anatomy.

study and how different experimental questions justify given collection strategies.

2.6.2 | It is in our blood; now, we need to find it

Many EM questions require extensive screening to locate evasive ROIs, a tedious and frustrating task made even more so if 3D information is required. Different correlative microscopy approaches address this problem, but a specific fluorescent signal is frequently unimportant and only a tool necessary to localise the elusive ROI in a larger context of the sample. Below, I use prepared blood cells to illustrate how AT-lateral screening helps to localise randomly distributed scarce structures of interest (Figure 3). The sample is a 'byproduct' of an HPF experiment and was not handled to enrich different cell types or achieve perfect image quality; indeed, the imperfection of the sample serves to highlight the efficiency of AT for lateral screening and ROI identification.

No special sample orientation efforts are required for sectioning a homogenous sample (Figure 3), and it can be directly set for trimming (Figure 3B). The sample was trimmed to a rectangular pyramid with enlarged sides, creating a 'ladder' with 50 µm steps (Figures 3B). This kind of trimming is rarely necessary for research samples, and here, the goal was to provide an example of how differently sized ribbons can be generated and transferred on the wafer while maintaining their relative sequence in order (Figure 3C and D). In the sequential collection, the first section will be at the lower part of the wafer, to the right. If acquired serially, the ribbons can be arranged one after another in a sequence (array) that advances from the bottom right to the top left (Figure 3D, arrows). In the example shown in Figure 3D, a depth of over 200 µm was covered: sequences of ~50 sections from alternating block levels were collected continuously, with the long portions in-between removed with an eyelash. This way, the ribbons on wafer have different widths that correspond to the width of the steps in the trimmed block.

A dry wafer is introduced into the SEM chamber to create the overall surface map using an in-microscope optic camera or automatically acquiring a sequence of tiled SEM images (Figure 3E). The resolution of these tiles already should be sufficient to get the general idea of ribbons position and their quality. They contain preliminary information regarding the quality of the sample and sectioning. Lateral screening and acquisition of selected sections provide immediate details on the distribution of different features of interest. When relevant ribbons are selected, the 'anchor' sections can be analysed with increased resolution (Figure 3F, anchors). For the representation of a particular feature on a section (e.g., several types of white cells), an intermediate-resolution (10 to 50 nm pixel) tiled image can be acquired (Figure 3G). Based on this targeted map, a precise ROIs can be attained with 2 to 5 nm pixel high resolution (Figure 3Gi–vi, highlighted in blue). If 3D information is required, the ROI can be collected sequentially from the adjacent sections and aligned into a stack (Figure 3H, Supplementary Movie 3a). However, frequently it is unnecessary, as even nonaligned sections provide plenty of ultrastructural information as is the case of thrombocyte presented in Figure 3I. If quantitative data are required, high-resolution tiles can be acquired. This large area can be analysed in detail after the acquisition since it can be magnified while preserving the overall reference space (Figure 3J, Supplementary Movie 3b). Such a dataset can be a reliable basis for quantitative analysis using stereology counts of different features on the entire section or its parts (Figure 3K).

2.6.3 | Retrieving information from a large area. No brainer!

Many aspects of neurobiology and brain studies heavily rely on EM analysis using multiple EM techniques spanning from single sections to impressive volumes. The priceless connectomic data and global studies has revealed numerous ultrastructural features of neurogenesis previously unavailable, to mention just a few.[34,35] Nevertheless, the effort required to obtain such large data volumes makes it an exception rather than an attainable standard. Even in neurobiology, few questions require the entire brain volume at the EM scale; more commonly, studies focus on the localisation of a feature of interest in this busy environment.

Even if a study is not attempting to capture the entire brain volume, TEM approaches are severely limited in the area that can be captured on a grid. Therefore, for many questions, AT is the most flexible approach. For example, the 100 µm thick slice of mouse hippocampus shown in Figure 4A can be sectioned in a serial (Figure 4Bi) or semiserial (Figure 4Bii) manner. Over 200 sections were collected on each wafer, and the decision to collect the ribbons randomly or sequentially depends on the project's actual needs.

If the experimental goal is to determine the distribution of small features from the sample, collecting information from a random section with high-resolution parameters 92 nm pixel size) might be a sound strategy (Figure 4C, arrow, and D). Multiple high-resolution tiles that compose the image can be observed in the overview mode and systematically zoomed in to allow the researcher to analyse small details. Though acquiring 400 tiles requires

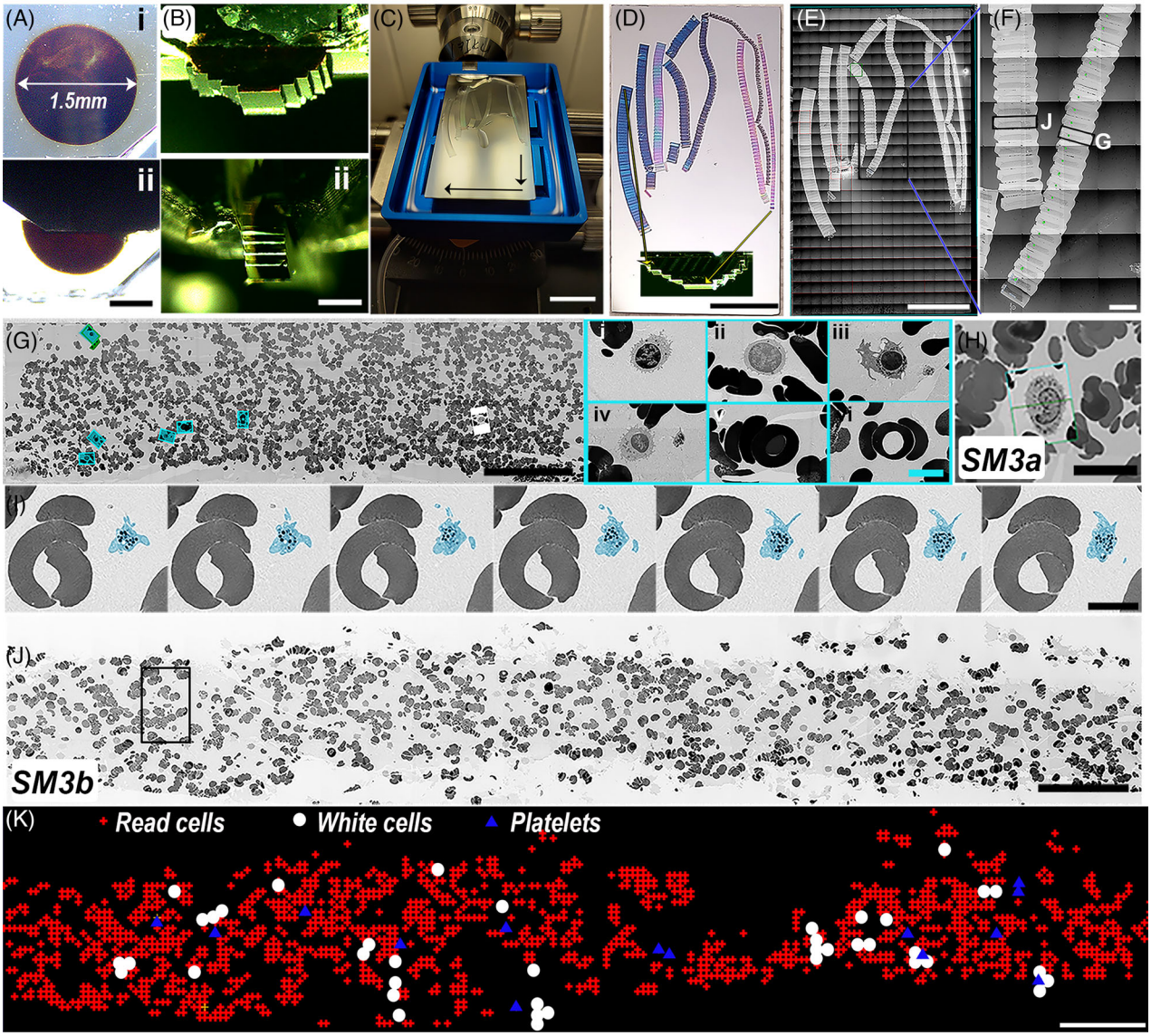

FIGURE 3 AT permits great flexibility for sample sectioning and array generation. (A) Flat block with a high-pressure freezing carrier containing blood-drop sample. i. Top view. ii. Same block pretrimmed with the razor blade set to the tweezer carrier of the Leica ultramicrotome. Scale bar: 1 mm. (B) Tight trimming of the sample aimed to follow the round shape of the sample. i. Each step in depth represents 50 μm, done for representation purposes. ii. Same block side view. Scale bar: 1 mm. (C) Top view on the ATS knife installed on ultramicrotome for intermittent sectioning of different block portions. The first collected section is at the bottom right, and the last is at the top left. Irrelevant ribbons were discarded during the sectioning using an eyelash. The sections are 100 nm on average. Scale bar: 1 cm. (D) A reflection image of a wafer with dry ribbons is an example of a sequence that can be created flexibly with a different 'breadth' of the sample, as per tiered trimming. The first and the last sections roughly correspond to the indicated positions on the block inset (arrows). Scale bar: 1 cm. (E) The same wafer was obtained with ETD-SE using Maps program tiles mode. The square grid on the image represents ~17 × 27 = 459 separate low-resolution tiles combined to create a wafer map. Usually, before stitching the image, seam marks between different tiles are visible. Scale bar: 1 cm. (F) The inset from panel E highlighting the areas selected for further analysis and the screen for potential ROI (Panels G and J). Scale bar: 1 mm. (G) A high-resolution (5 nm pixels) SEM tiled image acquired of region 'G' outlined with a black box in panel F provides sufficient resolution to…Zoom on one of the sections, relatively high zoom to define several rows. This resolution is enough to select the cells of interest. The regions in blue are zoomed in on several cells of interest. Different ROIs are in blue. Scale bar: 100 μm. Insets i–vi acquired with 3 to 5 nm pixel resolution. Scale bar: 10 μm. (H) A single slice from a sequence of serial images acquired by automated acquisition of multiple sections through a leucocyte using Maps program, aligned after using IMOD program. Segmenting the stack entirely or partially using the same program is possible. Scale bar: 10 μm. (I) Manually acquired sequence through a platelet, pseudo-coloured blue. Scale bar: 10 nm. (J) A high-resolution tiled image was acquired for detailed quantitative analysis off-microscope. After the stitching of different tiles into one image is complete, there are usually no visible seam marks. A black rectangular frame represents one of 168 separate 5 nm resolution images stitched into one. The image can be zoomed in on different regions to see the fine details of the sample. Scale bar: 100 μm. (K) A score map for stereological analysis of the cell populations from panel J was created with the IMOD. Red crosses – red blood cells, White rounds – white blood cells, Blue triangles – platelets. Scale bar: 100 μm.

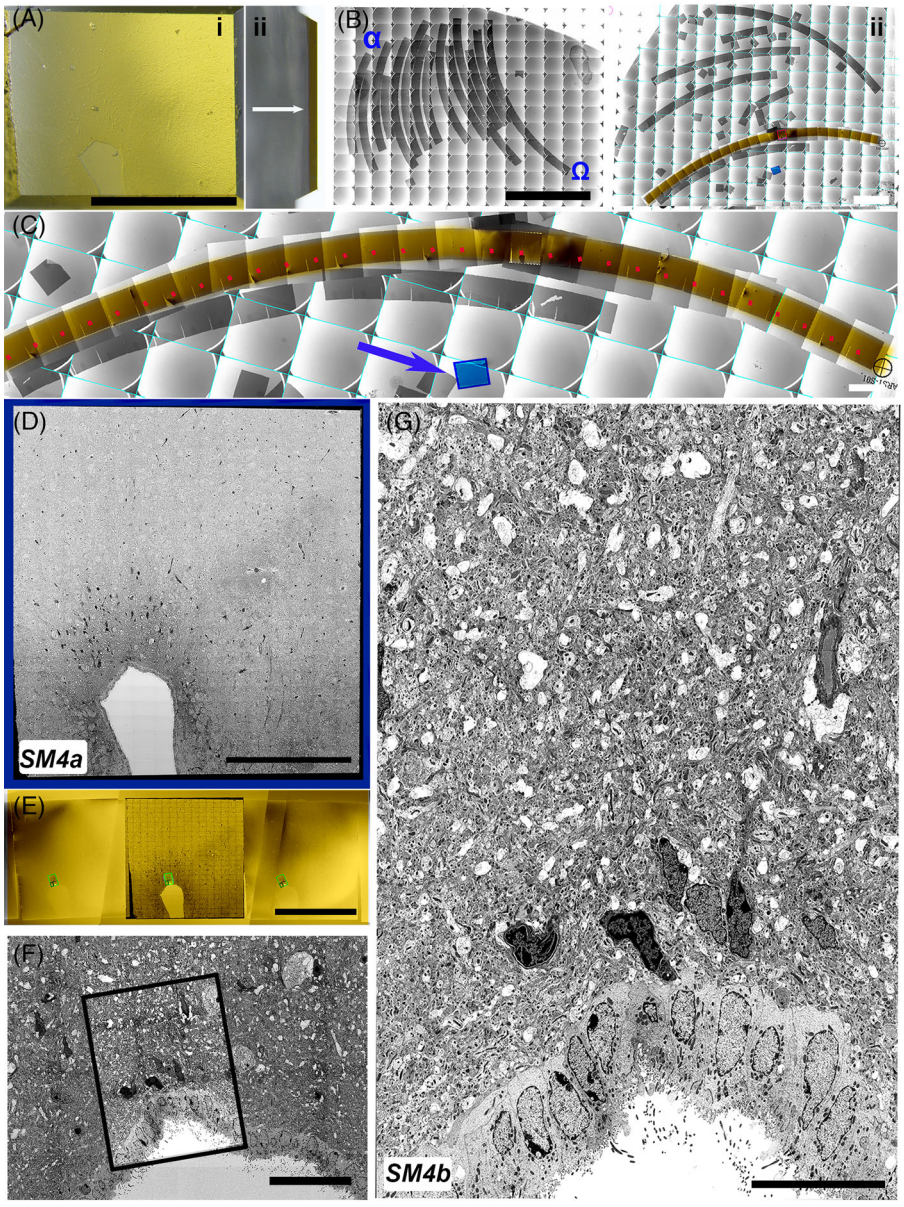

FIGURE 4 A vibratome slice of the mouse hippocampus was analysed with AT. (A) 100 μm vibratome slice of hippocampus embedded in HM20 embedded. Scale bar: 500 μm for both. i. Front view of the block from the part facing the knife. ii. Lateral view on the trimmed block. The arrow points to the vibratome section after sample preparation and embedding in resin. (B) Tiled images of two wafer acquired with ETD-SE. Scale bar: 1 cm. i. 200 serial sections collected on a wafer with. ȧ – first, Ȯ-last section. ii. 200 sections from the same sample were collected semirandomly. (C) A portion of the wafer from panel C features the ribbon of 25 serial sections (orange) and a single section (blue). Scale bar: 1 mm. (D) A tiled high-resolution image of the section from the entire surface of the block (Panel D, blue). Compare with Panel Ai. Scale bar: 300 μm. (E) A fraction of the orange ribbon sequence from panel D. The central image in the ribbon, collected as high-resolution tiles, similar to the image from panel E, to analyse and target a particular ROI for serial section imaging. Scale bar: 600 μm. (F) A portion of the image was delimited in panel F (yellow), which was selected to acquire a tiled image with *z* depth. The portion of the sample. Scale bar: 100 μm. (G) A high-resolution tiled image of one of the sections from the sequence of images aligned and represented in Supplementary Movie 4b. Scale bar: 50 μm.

several hours, unlike the 'live' observation in front of the SEM tool, the detailed analysis is done away from the microscope (Supplementary Movie 4a). If a 3D-volume from a particular region is required, acquiring a high-resolution tiled image of the entire section in *z* presents a challenge, time-consuming to acquire thus expensive, and difficult to analyse/manipulate, even using powerful computers. In addition, to address questions requiring high precision, multistitched image alignment is challenging to perform with precision and thus suboptimal. Instead, it

makes more sense to collect representative high-resolution information from the entire 'anchor' section of the ribbon (Figure 4C, orange, and E). After a detailed analysis of this image, one or several ROIs can be selected to collect at high-resolution (Figure 4F). The individual sections acquired for the *z* sequence can be aligned and analysed with or without segmentation (Figure 4G, Supplementary Movie 4b).

2.6.4 | How flat can it get: Dealing with monolayers

Monolayers of cultivated adherent cells are among the most challenging and error-prone samples to section. Usually, cells are grown at the bottom of the Petri dish/coverslip, typically ~10 μm in *z*, with the bulk of the cell volume containing the nucleus (Figure 5Ai). After processing and embedding for EM, the attached portion of the cell and its extensions end up directly at the surface of the block, with the bulk of the cells and their nuclei found deeper inside (Figure 5Aii). Only a tiny fraction of the flat embedded monolayer will be investigated (Figure 5B–D), with much of the surface trimmed during the preparation stage (Figure 5C – after preliminary razor blade trimming; Figure 5D, after final diamond trim). Localisation of the relevant ROI and perfect alignment of the entire embedded surface for ultracutting presents a significant challenge when dealing with cell monolayers. The ROI localisation for trimming and sectioning can be done by analysing the block's surface under the light microscope or correlating the fluorescence of a marker stain before or after the embedding. The orientation of this area parallel to the diamond knife blade heavily relies on the skill and patience of the operator, as it demands numerous iterations before the necessary parallelism can be achieved. If the parallelism is not attained, only a portion of the sample face will be sectioned initially (Figure 5E, illustration, and F, real sections). If sectioning continues, gradually, a larger proportion of the block face is sectioned until the entire sample depth will eventually be covered (Figure 5E and F). However, the sectioning plane on one side will feature a deeper portion of the sample, while the opposite part will contain sections very close to the surface (originally the coverslip support substrate).

Different from the challenges of the cell monolayer orientation and sectioning for TEM, preparation and analysis for AT render these issues less critical. The overall area of the processed monolayer tends to be larger in AT yet at the price of sacrificing perfect parallelism. Since AT enables the collection of the totality of sections, even if the sectioning does not produce neat ribbons, the subsequent recognition of the correct section sequence does not present a daunting task (Figure 5G; Supplementary Movie 5a). The first sections can be reliably identified merely on the progression of their relative size. Eventually, when the sections cover the entire block face and contain the data from the first section on, the correct sequence is evident either from the sequential arrangement or landmarks within the sample (Figure 5G).

It might appear counterintuitive, but recognising the ROI within the monolayer post-sectioning is easy, as sections have a visual imprint that can be understood when scrutinised. In many cases, it is often easier to begin the screening in the deeper part of the sample and *then* move outwards to the extremities. Even a portion of the data will provide sufficient information with a fraction of the effort and cost required for ssTEM or automatic vEM techniques (Figure 5H; Supplementary Movie 5b). With adherent cell monolayers, a limited *z*-depth is required to capture the entire volume (5–15 μm) depending on the cell type and experimental needs and therefore easily attainable using AT. If the whole volume is not essential, acquiring single large high-resolution 2D image from multiple sample regions can provide statistically reliable data.

2.6.5 | All about image quality and *z*: SEM detector deconvolution or how to cheat the system

The high resolution attainable by EM is the major strength of these techniques compared to other visualisation methods. Frequently, SEM-based techniques are presumed to have inferior resolution compared to TEM. Even though the statement is technically correct, this resolution is still superior to any optical method. Moreover, angstrom resolution is rarely required to address questions in cell biology. Indeed, the strength of AT is indisputable when a more global analysis of cells or tissues is required, primarily when a small, randomly scattered structure must be targeted in a large sample area/volume (Figure 6A; Supplementary Movie 6a).

The cristae inside the mitochondria, Golgi cisternae and MVB intraluminal vesicles are small and omnipresent structures that do not require large volumes, so they could be located reasonably easily and imaged using ssTEM or TEM tomography. Nevertheless, even in studies where TEM is traditionally a tool of choice, AT assessment can provide sufficient image quality and resolution as single images or 3D volumes (Figure 6B and C; Supplementary Movie 6b). The screening and analysis of smaller unicellular organisms, such as bacteria and yeast, can benefit from this approach for projects or diagnostics that require distinguishing between different populations, for

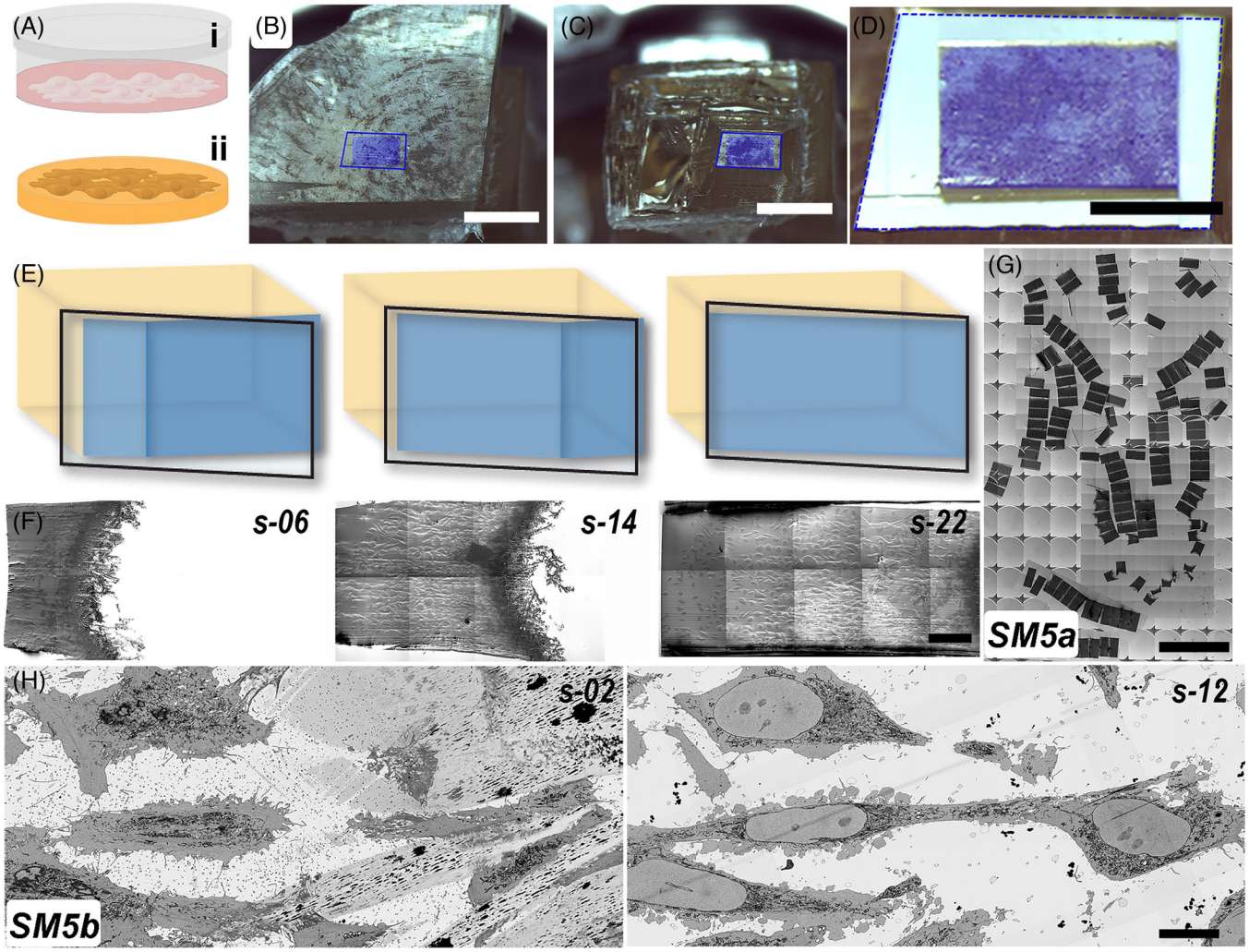

FIGURE 5 Cutting the monolayers of cells. (A) Schematic drawing of cultured monolayer cells in a Petri dish (i) and an embedded replica of the same sample (ii). At the end of the embedding procedure, the sample presents a mirror image replica of the cultivated lawn. (B) A fraction of a block with Hela cell monolayer embedded in Epon. The cells are cultivated on a glass coverslip, and a ¼ was mounted for sectioning. However, only a fraction of this fraction will eventually be prepared for ultrathin sectioning and the subsequent analysis. Blue line – the ROI hand trimming area, blue rectangle – the region dedicated to precision diamond trimming. Scale bar: 2 mm. (C) The same sample as in panel B after hand trimming with a razor blade, defining the ROI. Scale bar: 2 mm. (D) The block as in panel C, after trimming with is trimmed with 90° diamond-blade trimmer. Scale bar: 1 mm. (E) A schematic drawing of the sectioning plane orientation. Block face in blue. (F) A partially sectioned face of the sample. The left side already contains the sections, while the right side is still empty and incomplete. With the progression of sectioning deeper into the sample, the cell starts populating the entire area. Scale bar: 200 μm. (G) A composite map of a wafer covers the entire sectioned monolayer, with most sections not organised sequentially. However, the correct sequence can be easily identified, even without the guides, since the topography of the ultrastructure is usually apparent when closely studied. Scale bar: 5 mm. (H) Sections 2 and 12 from the putative ROI. Scale bar: 10 μm.

example, to characterise different populations of bacteria in the microbiome (Figure 6D).

The concept of 'energy deconvolution' was introduced in the last decade. In this method, the change in accelerating voltage is used to image into a depth of the SBF sample.[36] This way, even relatively thick SBF-SEM slices could increase isotropic resolution; unfortunately this powerful FEI technology is rarely accessible. AT sections are relatively thin, and it might not be the best strategy to invest the effort in changing the accelerating voltage for each section. However, there is a way to benefit from a similar approach by using multiple backscatter electron detectors. SEM microscopes can be equipped with multiple detectors, such as the BSE through-lens TLD or in-lens MD or ICD detectors (Figure 6E) that collect the scattered electrons from different sample depths, providing a slightly different image (Figure 6F). Using a particular combination of detectors without changing the accelerating voltage, they are bound to pick a signal from the lower levels of the section. The simultaneous acquisition by

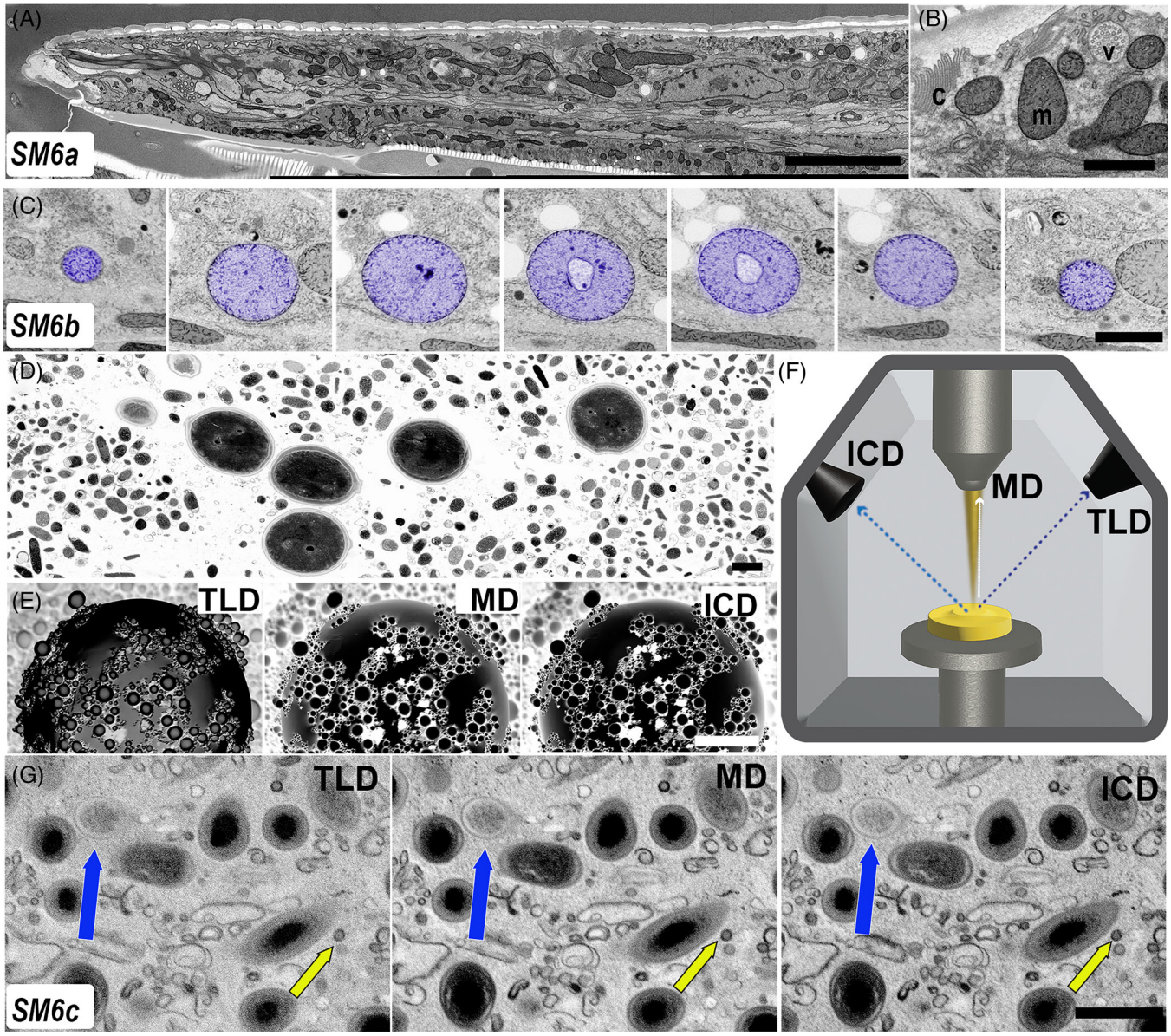

FIGURE 6 Image quality and multidetector acquisitions. (A) A part of a longitudinal section through the *C. elegans* head acquired as tiles, using the MD-BSE detector. Tiles of images acquired at 3 nm pixel size resolution (punctured lines define separate image tiles). Each portion of the image is informative with very high precision. Each portion can be acquired in 3D as part of the image sequence. Scale bar: 5 μm. (B) An MD-BSE detector image of the portion of a section through *C. elegans* epidermis showing the mitochondria (m), MVB (v), and membranous cristae (c). The yield of SEM resolution of 5 nm pixel size for such an image cannot be told apart from an equivalent image obtained with a classic TEM image. Scale bar: 1 μm. (C) A sequence of the atypical mitochondrion acquired in 3D and pseudo-coloured blue. The image's resolution is comparable with TEM and sufficient for many studies concentrating on organelle structure. Scale bar: 1 μm. (D) A portion of the image from the *C. elegans* experiment featuring *E. coli* bacteria and baker's yeast was used as a cryoprotectant during the high-pressure freezing experiments. The image's resolution is sufficient to distinguish between two organisms and the quality of their preservation. Scale bar: 1 μm. (E) A schematic drawing of the SEM chamber with different detectors inside. The emitted scattered electrons are collected simultaneously by all three detectors. (F) A calibration tin balls specimen was acquired simultaneously with a transmission light (TLD), mirror (MD), and in-column (ICD) BCE detectors. The resulting image is slightly different from one another. Scale bar: 1 μm. (G) A random ROI of the *E. coli* sample was acquired simultaneously with three detectors. Arrows indicate subtle differences discernible on static sections. More details are visible in the sequence of Supplementary Movie 6c. Scale bar: 1 μm.

different detectors, performed on several sequential sections, provides additional in-depth information for thicker sections (Figure 6G, arrows). Even though it does not provide information about the precise depth of the sections, it adds details to smaller features and reveals sharper and more uniform 3D information (evident in Supplementary Movie 6c).

2.6.6 | Detangling the ravel: Glomeruli for beginners

Ultrastructural information is required to diagnose diseases like ciliopathies, kidney, intestinal and lung problems. Biopsy analyses are regularly performed in medical centres' EM service or pathology departments to deliver a definitive diagnosis. Obtaining conclusive results rapidly and from every sample is crucial, as they are unique, cannot be easily repeated, and frequently the results define the course of treatment for the patient. Unfortunately, biopsy samples are usually transferred from the operation theatre to the pathology/EM facility without carefully considering sample quality or orientation, making the processing even more challenging. The samples are prepared by standard chemical fixation with osmium contrast and Epon-based embedding, and the quality of such a resin-based EM sample can only be determined once analysed. On the plus side, the primary goal of these tests is to achieve a high-fidelity answer from a relevant region rather than a high-quality image.

Kidney diseases are among those that require EM for final diagnosis or to assess the organ condition before or after transplantation. The state of glomeruli and the intactness of the Bowman capsule are used to evaluate blood filtration capacity. The workflow below shows a mouse kidney as an example of glomeruli analysis or similar diagnostic approaches. Routinely, kidney sample preparation involves iterations of semithin sectioning and toluidine blue staining until the ROI is reached. Then several thin sections are transferred to grids for further EM analysis. There is no easy way to determine sample quality before the final step of the TEM assessment. However, on its own, the preceding manipulations have no informative value as information is not retained and are a time-consuming, destructive procedure.

Using the AT approach, samples can be directly sectioned to rapidly generate 50–100 thin large sections (Figure 7A). With the sections collected as arrays, this number of sections likely contains the target structures, such as glomeruli. In addition, portions of the sample can be collected with different section thicknesses covering a more extensive volume depth, increasing the chance of securing the ROI or sampling an even more significant portion of the biopsy. If needed, lateral screening will rapidly produce enough candidates for in-depth quantitative analysis. Low-magnification images, within the resolution relevant for each structure type, can localise the appropriate structures without requiring lengthy acquisitions (Figure 7B). Once identified, the ROI can be imaged at higher resolution as single tiled images of the entire structure (Figure 7C) or its parts (Figure 7D). If the structure of interest is not easily discernible in rapid screening, it makes sense to acquire high-resolution tiles from several sections and screen them carefully off-microscope (Figure 7E; Supplementary Material 7a). With knowledge of the potential ROI distribution, a reliable acquisition routine can be generated for each diagnostic question. Even though there is no need for 3D in the majority of the current diagnostic questions, it might open a possibility for novel types of diagnostic screening.

3 | DISCUSSION

3.1 | How to increase analysis by ultrastructure for research and diagnostics?

Unfortunately, the fundamental technological revolution related to transitioning from TEM imaging to SEM to acquire information inside the cell has not been generally appreciated until recently.[2] Modern SEM technologies can revolutionise the way electron microscopy can impact biological research, potentially substitute TEM for a lion share of cell and tissue analysis studies in bioresearch and medicine. Multiple examples of SEM-based methods (SBF, FIB, or AT) provide solid scientific data and show a strong potential for change in the field. This leap in technology has been matched by the progress in SEM-based sample preparation methodology, and even though the expertise and equipment are not new, the SEM-based approaches have yet to be utilised to the full extent.

Frequently, a conceptual mistake consists of treating the totality of a given EM approach as one global concept from the beginning of the procedure until its end. The success or the failure to achieve a desired result is attributed to a technique as a whole. Instead, it should be considered as several independent steps that, if successfully combined, provide the required results. The steps of sample preparation, image acquisition, analysis of observations, data alignment and segmentation of the datasets are unrelated steps with a subset of variable constraints for each. Even though each failing step can negatively impact another step or the entire procedure, each part of the workflow has unique strong and weaker points to be addressed separately.

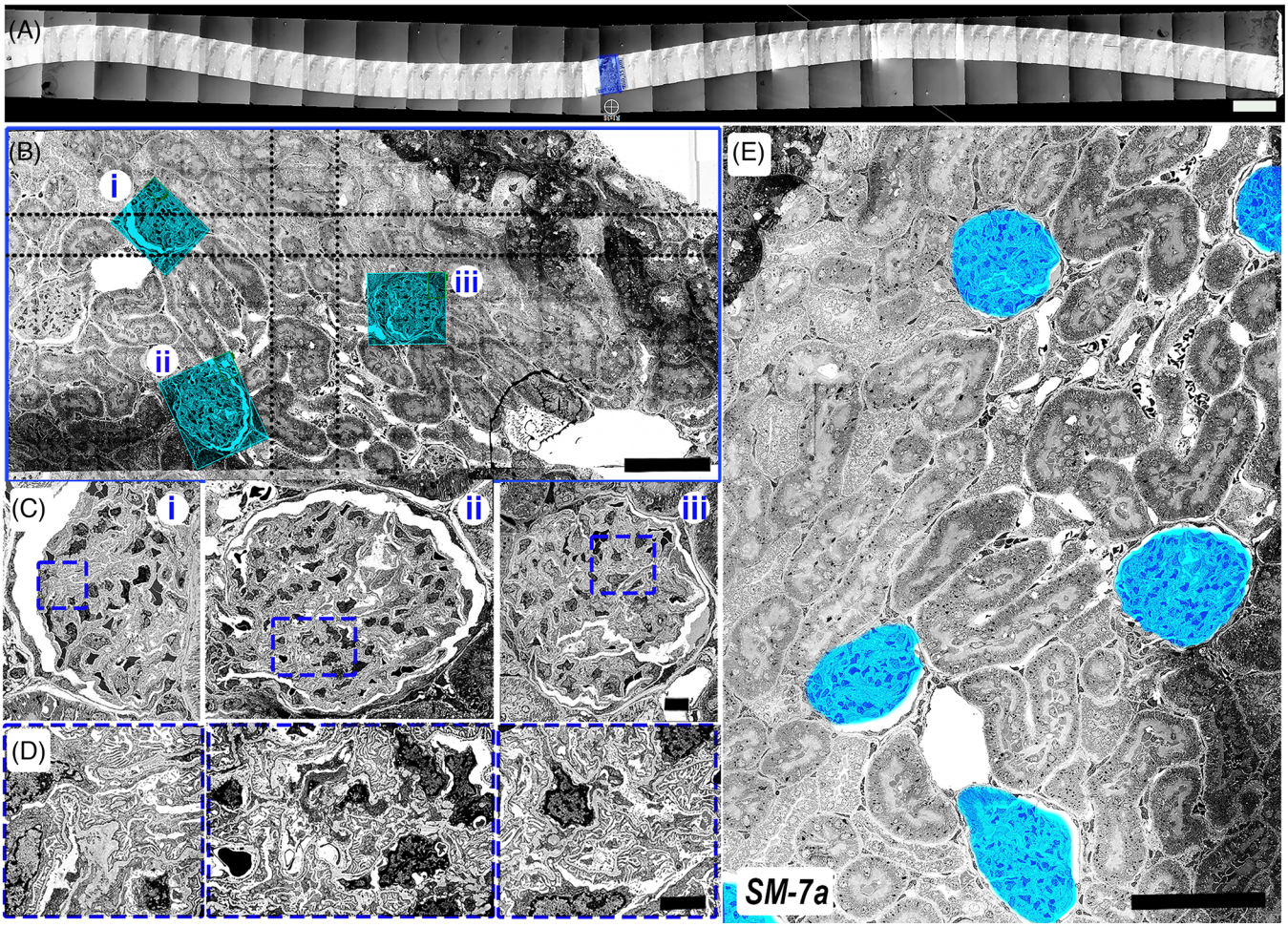

FIGURE 7 Kidney glomeruli and the quest for rapid sample analysis. (A) A portion of a tiled SE-ECD image is a ribbon of 50 sequential rat kidney sections of 2.15×1.30 mm block face. A central section (blue) was chosen for the 'anchor' analysis. When selected in this section, an ROI can be collected in 3D following the upstream and downstream located sections. Scale bar: 1 mm. (B) A tiled BSE-MD image of the entire blue section from panel A, collected at a midrange 20 nm pixel size. This resolution is already sufficient to recognise the glomeruli (i-iii, blue) without further need to improve the acquisition strategy and spend more time on acquisition. Scale bar: 100 μm. (C) Tiled SEM-MD images of the cross-section through three different glomeruli (i–iii) acquired at 5 nm pixel. The resolution provides the necessary information regarding the state of the podocytes (i–iii). Scale bar: 10 μm. (D) The entire image or its portions can be acquired with even higher resolution (3 nm pixel), as shown by concentrating on yellow insets. Scale bar: 5 μm (E) An entire section acquired with high resolution can be zoomed in on any portion when observed off-microscope. This way, an overall view of a larger area and detailed information about each part are accessible in one dataset and suitable for stereological clinical quantification. Scale bar: 100 μm.

Another problem is that different SEM-related techniques are considered mainly in the context of vEM. This is understandable as SBF and FIB have pioneered the field by providing extensive TEM-like 3D data with apparent ease compared to the ssTEM. An underappreciated and widely applicable advantage of SEM imaging is the ability to create large 2D high-resolution maps of biological anatomy, which on their own can provide unprecedented valuable information while retaining context. However, the same enthusiasm likely limited the use of SEM for non-vEM approaches. For example, projects that benefit from an extensive volume provided by SBF or superior *z* resolution provided by FIB represent only a fraction of the total cases where ultrastructural data is required.[37] Such global studies aimed to generate atlases and reference databases accessible to the large scientific communities are the one-time effort of large groups and should not be treated as representative . Furthermore, when operating costs make the use of technology unachievable financially (frequently the case with large datasets), the possibility of using the approach is often not considered by less 'financially plentiful' labs. Because AT utilises equipment that is often already on hand, this approach is more accessible to researchers and clinicians at various facilities.

Although the novel SEM technologies have not initiated the EM revolution that might have been predicted

some 20 years ago, AT could rectify the situation. AT allows the microscopist to concentrate on the relevant ROIs and reimage several areas without the problems of contrast, charging and data oversampling compared to other techniques. Compared to other vEM, it is easy to master, and the learning curve is much shallower. Furthermore, since the FOV is no longer limited, various problems and artefacts seen in TEM experiments are no longer an issue. Thus, AT can successfully substitute for TEM for any application requiring over 2 nm scanning pixel size resolution. The same preparation technique can also be used for histology, in combination with immuno-correlative and multiplex fluorescent microscopy and immuno-gold labelling, further expanding its potential.

With all its benefits, image alignment is the primary disadvantage of AT compared with FIB and SBF EM. In this respect, AT is reminiscent of ssTEM problems caused by distortion and the need to align variably oriented images. Several programs (freeware and commercial) are available for this need, yet their efficiency dramatically depends on the sample type.[38–41] This might be a genuine consideration for questions requiring thousands of sections/large volumes or a very small z to obtain isotropic information. However, for many questions, even an imperfect z stack can provide valuable information and 3D context without the need for 3D rendering. Automatic acquisition is frequently considered a positive and beneficial distinction from destructive methods. Successful attempts are made to make AT competitive in this domain, with different applications localising the ROIs and systematically collecting the sequence of the sections without operator interference. As with other aspects, the acquisition mode will depend on the goals, as for numerous applications, semiautomation or no automation at all represent a more straightforward approach altogether.

The steps related to AT analysis make it extremely prone to interactive collaborations as different steps do not have to be performed in one place or by one team.

- -Wafers are robust and can be shipped between facilities without problems
- -More and more modern EM tools can be operated in distance mode
- -Versatile analysis of the data can be done without the need to have an on-site specialist. This division can significantly speed up the workflow.
- -Sectioning can be done even as part of the histopathology facility, as the adaptation of the skills between microtomy and ultramicrotomy is minimal.
- -Mutant screens are routinely performed by LM; however, AT makes it possible to perform ultraresolution screens, opening the potential for many overlooked problems on the cellular level.
- -Each 3D dataset can be segmented, and the central limit in how detailed and ample this segmentation is will depend only on the sheer time one is willing to spend on the task. Even with AI algorithms, the extent of the workforce will eventually define the attained complexity. The good news is that very little training is required for this step, and it can be performed even by individuals entirely untrained in biology with little to no understanding of the system.[42]

Beyond basic research, EM holds great potential for medical diagnostics. Histology, transmission light, and fluorescence microscopy methods are widely used in medicine. TEM is used to detect different ciliopathies, kidney and digestive system diseases together with several other conditions challenging to detect by other means. However, the use of the modern EM approaches is infrequent in diagnostics, albeit a number of impressive publications recently, to mention a few.[43–47] Several reasons exist, including processing time and the need for rare expertise. AT can solve a significant problem in many diagnostic institutions: the analysis can be performed in multiple facilities. The EM facility staff member is usually responsible for sample preparation and image generation. Therefore, if either specialist is unavailable on-site, the entire diagnostic procedure becomes unavailable to patients at this facility. The use of AT can eliminate many time-consuming intermediate steps and can allow staff at one facility to prepare the sample, and the resulting wafers (or imaging data) can be transferred to another facility for imaging (or interpretation). This workflow can increase access to accurate diagnostic screening without requiring all necessary equipment at one site.

Modern SEM can potentially substitute for TEM for most diagnostic tasks, making analysis more accessible and widespread. Moreover, the reduced complexity of the SEM procedures and acquisitions can help diagnose established diseases and holds a great potential to identify or characterise new ones that can only be detected with large area or 3D access to the ultrastructure.

4 | CONCLUSION: THE REAL POWER OF AT IS NOT A VEM FOR THE POOR! IT IS AN EASY TEM AND VEM FOR ALL!

Even after many years of successfully demonstrating its different benefits, EM still needed to become the standard tool for life science analysis. In this article, I present a range of biological samples and several questions that illustrate

the benefits of AT-SEM. Combined with previously published studies, it demonstrates how the technique could be applied to almost any research system within a reasonable effort-to-result ratio. For those who consider using AT, there are several scenarios for when AT may be preferable:

Too tedious for TEM
The resolution of 2 nm pixel size is sufficient for a given ROI
Too long to set the procedure for SBF/FIB acquisition
The z range is between 50 and 500 sections
A relatively large FOV is required
The need to screen multiple samples/experimental conditions
A need to re-acquire the ROI with different parameters
Need to analyse several FOVs in the same sample

Array Tomography is a simplified EM approach that can produce results faster than any other technique for samples meeting the abovementioned criteria and constrains.

ACKNOWLEDGEMENTS

I am grateful to my colleagues Lindsay Lewellyn, Gareth Griffiths, Tilman Franke, Christel Genoud, Helmut Gnaegi, Max Heiman and Jemima Burden for constructive comments on the manuscript.

Open access funding provided by Universite de Lausanne.

ORCID

Irina Kolotuev https://orcid.org/0000-0003-1433-8048

REFERENCES

1. Peddie, C. J., Genoud, C., Kreshuk, A., Meechan, K., Micheva, K. D., Narayan, K., Pape, C., Parton, R. G., Schieber, N. L., Schwab, Y., Titze, B., Verkade, P., Aubrey, A., & Collinson, L. M. (2022). Volume electron microscopy. *Nature Reviews Methods Primers*, *2*, 51.
2. Collinson, L. M., Bosch, C., Bullen, A., Burden, J. J., Carzaniga, R., Cheng, C., Darrow, M. C., Fletcher, G., Johnson, E., Narayan, K., Peddie, C. J., Winn, M., Wood, C., Patwardhan, A., Kleywegt, G. J., & Verkade, P. (2023). Volume EM: A quiet revolution takes shape. *Nature Methods*, *20*, 777–782.
3. Denk, W., & Horstmann, H. (2004). Serial block-face scanning electron microscopy to reconstruct three-dimensional tissue nanostructure. *PLoS Biology*, *2*, e329.
4. Knott, G., Marchman, H., Wall, D., & Lich, B. (2008). Serial section scanning electron microscopy of adult brain tissue using focused ion beam milling. *Journal of Neuroscience*, *28*, 2959–2964.
5. Kizilyaprak, C., Daraspe, J., & Humbel, B. M. (2014). Focused ion beam scanning electron microscopy in biology. *Journal of Microscopy*, *254*, 109–114.
6. Micheva, K. D., & Smith, S. J. (2007). Array tomography: a new tool for imaging the molecular architecture and ultrastructure of neural circuits. *Neuron*, *55*, 25–36.
7. Micheva, K. D., Busse, B., Weiler, N. C., O'Rourke, N., & Smith, S. J. (2010a). Single-synapse analysis of a diverse synapse population: Proteomic imaging methods and markers. *Neuron*, *68*, 639–653.
8. Oberti, D., Kirschmann, M. A., & Hahnloser, R. H. (2011). Projection neuron circuits resolved using correlative array tomography. *Frontiers in Neuroscience*, *5*, 50.
9. Horstmann, H., Korber, C., Satzler, K., Aydin, D., & Kuner, T. (2012). Serial section scanning electron microscopy (S3EM) on silicon wafers for ultra-structural volume imaging of cells and tissues. *PLoS ONE*, *7*, e35172.
10. Hayworth, K. J., Morgan, J. L., Schalek, R., Berger, D. R., Hildebrand, D. G., & Lichtman, J. W. (2014). Imaging ATUM ultrathin section libraries with WaferMapper: a multi-scale approach to EM reconstruction of neural circuits. *Frontiers in Neural Circuits*, *8*, 68.
11. Kasthuri, N., Hayworth, K. J., Berger, D. R., Schalek, R. L., Conchello, J. A., Knowles-Barley, S., Lee, D., Vazquez-Reina, A., Kaynig, V., Jones, T. R., Roberts, M., Morgan, J. L., Tapia, J. C., Seung, H. S., Roncal, W. G., Vogelstein, J. T., Burns, R., Sussman, D. L., Priebe, C. E., … Lichtman, J. W. (2015). Saturated reconstruction of a volume of neocortex. *Cell*, *162*, 648–661.
12. Varsano, N., & Wolf, S. G. (2022). Electron microscopy of cellular ultrastructure in three dimensions. *Current Opinion in Structural Biology*, *76*, 102444.
13. Radulovic, S., Sunkara, S., Rachel, R., & Leitinger, G. (2022). Three-dimensional SEM, TEM, and STEM for analysis of large-scale biological systems. *Histochemistry and Cell Biology*, *158*, 203–211.
14. Peddie, C. J., & Collinson, L. M. (2014). Exploring the third dimension: Volume electron microscopy comes of age. *Micron (Oxford, England: 1993)*, *61*, 9–19.
15. Kubota, Y., Sohn, J., & Kawaguchi, Y. (2018). Large volume electron microscopy and neural microcircuit analysis. *Frontiers in Neural Circuits*, *12*, 98.
16. Wacker, I., Spomer, W., Hofmann, A., Thaler, M., Hillmer, S., Gengenbach, U., & Schroder, R. R. (2016). Hierarchical imaging: A new concept for targeted imaging of large volumes from cells to tissues. *BMC Cell Biology [Electronic Resource]*, *17*, 38.
17. Templier, T. (2019). MagC, magnetic collection of ultrathin sections for volumetric correlative light and electron microscopy. *Elife*, *8*, e45696.
18. Koike, T., Kataoka, Y., Maeda, M., Hasebe, Y., Yamaguchi, Y., Suga, M., Saito, A., & Yamada, H. (2017). A device for ribbon collection for array tomography with scanning electron microscopy. *Acta Histochemica et Cytochemica*, *50*, 135–140.
19. Burel, A., Lavault, M. T., Chevalier, C., Gnaegi, H., Prigent, S., Mucciolo, A., Dutertre, S., Humbel, B. M., Guillaudeux, T., & Kolotuev, I. (2018). A targeted 3D EM and correlative microscopy method using SEM array tomography. *Development (Cambridge, England)*, *145*, dev160879.
20. White, I. J., & Burden, J. J. (2023). A practical guide to starting SEM array tomography – An accessible volume EM technique. *Methods in Cell Biology*, *177*, 171–196.

21. Galenza, A., Moreno-Roman, P., Su, Y. H., Acosta-Alvarez, L., Debec, A., Guichet, A., Knapp, J. M., Kizilyaprak, C., Humbel, B. M., Kolotuev, I., & O'Brien, L. E. (2023). Basal stem cell progeny establish their apical surface in a junctional niche during turnover of an adult barrier epithelium. *Nature Cell Biology*, *25*, 658–671.
22. Fung, W., Tan, T. M., Kolotuev, I., & Heiman, M. G. (2023). A sex-specific switch in a single glial cell patterns the apical extracellular matrix. *BioRxiv*.
23. Santella, A., Kolotuev, I., Kizilyaprak, C., & Bao, Z. (2022). Cross-modality synthesis of EM time series and live fluorescence imaging. *Elife*, *11*, e77918.
24. Rohrbach, A., Caron, E., Dali, R., Brunner, M., Pasquettaz, R., Kolotuev, I., Santoni, F., Thorens, B., & Langlet, F. (2021). Ablation of glucokinase-expressing tanycytes impacts energy balance and increases adiposity in mice. *Molecular Metabolism*, *53*, 101311.
25. Pasquettaz, R., Kolotuev, I., Rohrbach, A., Gouelle, C., Pellerin, L., & Langlet, F. (2021). Peculiar protrusions along tanycyte processes face diverse neural and nonneural cell types in the hypothalamic parenchyma. *Journal of Comparative Neurology*, *529*, 553–575.
26. Kato, M., Kolotuev, I., Cunha, A., Gharib, S., & Sternberg, P. W. (2021). Extrasynaptic acetylcholine signaling through a muscarinic receptor regulates cell migration. *Pnas USA*, *118*(1), e1904338118.
27. Franke, T., & Kolotuev, I. (2021). Array tomography workflow for the targeted acquisition of volume information using scanning electron microscopy. Journal of visualized experiments: JoVE. https://doi.org/10.3791/61847
28. Nikolaev, M., Mitrofanova, O., Broguiere, N., Geraldo, S., Dutta, D., Tabata, Y., Elci, B., Brandenberg, N., Kolotuev, I., Gjorevski, N., Clevers, H., & Lutolf, M. P. (2020). Homeostatic mini-intestines through scaffold-guided organoid morphogenesis. *Nature*, *585*, 574–578.
29. Kolotuev, I., & Micheva, K. D. (2019). Can correlative microscopy ever be easy? An array tomography viewpoint. In: P. Verkade & L. Collinson (Eds.), *Correlative imaging*. Wliey.
30. Micheva, K. D., O'Rourke, N., Busse, B., & Smith, S. J. (2010b). Array tomography: rodent brain fixation and embedding. Cold Spring Harbor Protocols, *2010*, pdb prot5523.
31. Tapia, J. C., Kasthuri, N., Hayworth, K. J., Schalek, R., Lichtman, J. W., Smith, S. J., & Buchanan, J. (2012). High-contrast en bloc staining of neuronal tissue for field emission scanning electron microscopy. *Nature Protocols*, *7*, 193–206.
32. Wacker, I., & Schroeder, R. R. (2013). Array tomography. *Journal of Microscopy*, *252*, 93–99.
33. Kolotuev, I. (2014). Positional correlative anatomy of invertebrate model organisms increases efficiency of TEM data production. *Microscopy and Microanalysis*, *20*, 1392–1403.
34. Swanson, L. W., & Lichtman, J. W. (2016). From cajal to connectome and beyond. *Annual Review of Neuroscience*, *39*, 197–216.
35. Xu, C. S., Hayworth, K. J., Lu, Z., Grob, P., Hassan, A. M., Garcia-Cerdan, J. G., Niyogi, K. K., Nogales, E., Weinberg, R. J., & Hess, H. F. (2017). Enhanced FIB-SEM systems for large-volume 3D imaging. *Elife*, *6*, e25916.
36. de Goede, M., Johlin, E., Sciacca, B., Boughorbel, F., & Garnett, E. C. (2017). 3D multi-energy deconvolution electron microscopy. *Nanoscale*, *9*, 684–689.
37. Heinrich, L., Bennett, D., Ackerman, D., Park, W., Bogovic, J., Eckstein, N., Petruncio, A., Clements, J., Pang, S., Xu, C. S., Funke, J., Korff, W., Hess, H. F., Lippincott-Schwartz, J., Saalfeld, S., Weigel, A. V., & Team, C. P. (2021). Whole-cell organelle segmentation in volume electron microscopy. *Nature*, *599*, 141–146.
38. Kremer, J. R., Mastronarde, D. N., & McIntosh, J. R. (1996). Computer visualization of three-dimensional image data using IMOD. *Journal of Structural Biology*, *116*, 71–76.
39. Cardona, A., Saalfeld, S., Schindelin, J., Arganda-Carreras, I., Preibisch, S., Longair, M., Tomancak, P., Hartenstein, V., & Douglas, R. J. (2012). TrakEM2 software for neural circuit reconstruction. *PLoS ONE*, *7*, e38011.
40. Belevich, I., Joensuu, M., Kumar, D., Vihinen, H., & Jokitalo, E. (2016). Microscopy image browser: A platform for segmentation and analysis of multidimensional datasets. *PLoS Biology*, *14*, e1002340.
41. Garza-Lopez, E., Vue, Z., Katti, P., Neikirk, K., Biete, M., Lam, J., Beasley, H. K., Marshall, A. G., Rodman, T. A., Christensen, T. A., Salisbury, J. L., Vang, L., Mungai, M., AshShareef, S., Murray, S. A., Shao, J., Streeter, J., Glancy, B., Pereira, R. O., … Hinton, A. Jr. (2021). protocols for generating surfaces and measuring 3D organelle morphology using Amira. *Cells*, *11*(1), 65.
42. Spiers, H., Songhurst, H., Nightingale, L., de Folter, J., Zooniverse Volunteer, C., Hutchings, R., Peddie, C. J., Weston, A., Strange, A., Hindmarsh, S., Lintott, C., Collinson, L. M., & Jones, M. L. (2021). Deep learning for automatic segmentation of the nuclear envelope in electron microscopy data, trained with volunteer segmentations. *Traffic (Copenhagen, Denmark)*, *22*, 240–253.
43. Eckly, A., Rinckel, J. Y., Proamer, F., & Gachet, C. (2018). High-resolution 3D imaging of megakaryocytes using focused ion beam-scanning electron microscopy. *Methods in Molecular Biology*, *1812*, 217–231.
44. Reichelt, M., Sagolla, M., Katakam, A. K., & Webster, J. D. (2020). Unobstructed multiscale imaging of tissue sections for ultrastructural pathology analysis by backscattered electron scanning microscopy. *Journal of Histochemistry and Cytochemistry*, *68*, 9–23.
45. Antao, N. V., Lam, C., Davydov, A., Riggi, M., Sall, J., Petzold, C., Liang, F. X., Iwasa, J., Ekiert, D. C., & Bhabha, G. (2023). 3D reconstructions of parasite development and the intracellular niche of the microsporidian pathogen *E. intestinalis*. bioRxiv.
46. Inoue, T., Ohno, N., Oishi, N., Mochizuki, K., Katoh, R., & Kondo, T. (2023). Three-dimensional structural analysis of papillary thyroid carcinoma nuclei with serial block-face scanning electron microscopy (SBF-SEM). *Pathology International*, *73*(8), 341–350.
47. Honda, K., Takaki, T., & Kang, D. (2023). Recent advances in electron microscopy for the diagnosis and research of glomerular diseases. *Kidney Research and Clinical Practice*, *42*, 155–165.
48. Yin, W., Brittain, D., Borseth, J., Scott, M. E., Williams, D., Perkins, J., Own, C. S., Murfitt, M., Torres, R. M., Kapner, D., Mahalingam, G., Bleckert, A., Castelli, D., Reid, D., Lee, W. A., Graham, B. J., Takeno, M., Bumbarger, D. J., Farrell, C., … da Costa, N. M. (2020). A petascale automated imaging pipeline for mapping neuronal circuits with high-throughput transmission electron microscopy. *Nature Communications*, *11*, 4949.

SUPPORTING INFORMATION

Additional supporting information can be found online in the Supporting Information section at the end of this article.

How to cite this article: Kolotuev, I. (2024). Work smart, not hard: How array tomography can help increase the ultrastructure data output. *Journal of Microscopy*, *295,* 42–60. https://doi.org/10.1111/jmi.13217